Available online at www.sciencedirect.com
SCIENCE DIRECT®
Biochemical and Biophysical Research Communications 304 (2003) 73–77
BBRC
www.elsevier.com/locate/ybbrc

The 3D structure of rat DPPIV/CD26 as obtained by cryo-TEM and single particle analysis

Kai Ludwig,[a] Shuling Yan,[b] Hua Fan,[b] Werner Reutter,[b] and Christoph Böttcher[a,*]

[a] *Forschungszentrum für Elektronenmikroskopie, Freie Universität Berlin, Fabeckstr. 36a, D-14195 Berlin-Dahlem, Germany*
[b] *Institut für Molekularbiologie und Biochemie, Fachbereich Humanmedizin, Freie Universität Berlin, Arnimallee 22, D-14195 Berlin-Dahlem, Germany*

Received 14 March 2003

Abstract

We present the three-dimensional structure of rat DPPIV/CD26, as determined by cryo-TEM and single particle analysis at a resolution of ~14 Å. The reconstruction confirms that the protein exists as a dimer, as predicted earlier. Since there are structural analogies to the serine peptidase POP, docking calculations of the two structures were performed. Although the docking showed a similar spatial organization (catalytic domain, β-propeller, distal opening, central cavity), the detailed comparison revealed clear discrepancies. The most marked difference is a second (lateral) opening in DPPIV/CD26, which would enable direct access to the catalytic site. We therefore assume that substrate selectivity and binding rate are most probably driven by different mechanisms in DPPIV/CD26 and POP.

Keywords: Dipeptidyl peptidase IV; CD26; Cryo-TEM; 3D-reconstruction; Single particle analysis

The serine protease dipeptidyl peptidase IV (DPPIV, CD26) (EC 3.4.14.5) is a widely distributed type II plasma membrane glycoprotein, expressed as a non-covalently linked 210 kDa homodimer at the cell surface of nearly all mammalian tissues [1]. This protein is a multifunctional protein, involved in a multitude of different biological processes [2]. Besides its role in immunoregulation and T cell activation [3,4], its peptidase activity is of particular interest: as an exopeptidase it cleaves N-terminal dipeptides from polypeptides with either proline or alanine residues in the penultimate position, thus regulating the function and activity of some peptide hormones and neuropeptides [5]. To understand the enzymatic mechanism of DPPIV/CD26, it is necessary to know its three-dimensional structure.

DPPIV/CD26 is highly conserved among different species. cDNA-sequences encoding human, mouse, and rat DPPIV/CD26, show 84.9% similarity [6,7]. The primary structure of rat DPPIV/CD26 consists of 767 amino acid residues. The N-terminus of this protein serves both as signal peptide and membrane anchor, containing a short cytoplasmic domain of six and a hydrophobic transmembrane domain of 22 amino acid residues [8]. The large extracellular domain of DPPIV/CD26 (739 amino acids) can be divided into three regions with specific characteristics. Adjacent to the membrane domain is the *N*-glycan-rich region containing 5 out of 8 N-glycosylation sites. The *N*-glycans of DPPIV/CD26 are essential for folding and biological stability of this molecule [9,10]. The central cysteine-rich region contains 10 of the 12 cysteine residues involved in the disulfide bridge formation necessary for the functional conformation of DPPIV/CD26 [11]. The C-terminus harbors the active site of this enzyme, which consists of a triad of amino acids including Ser^{631}, Asp^{709}, and His^{741} [12,13].

In this work we present the three-dimensional structure of rat DPPIV/CD26 determined by cryo-TEM and single particle analysis.

Materials and methods

Purification and isolation of homogeneous dimeric DPPIV/CD26 with enzymatic activity. cDNA of rat DPPIV/CD26 was cloned into the

* Corresponding author. Fax: +49-30-838-56589.
E-mail address: bottcher@chemie.fu-berlin.de (C. Böttcher).

0006-291X/03/$ - see front matter © 2003 Elsevier Science (USA). All rights reserved.
doi:10.1016/S0006-291X(03)00539-4

pRc/CMV expression vector (Invitrogen) and the recombinant plasmid DNA was transfected into CHO cells. Stable transfectants were selected, cloned, and characterized as described previously [9].

Enzymatically active DPPIV/CD26 was purified by immunoaffinity chromatography as described previously [14] with the following modifications: (1) the monoclonal anti-rat DPPIV mAb 13.4 was covalently coupled to a protein A–Sepharose Cl 4B column (Sigma, P3391) for the affinity chromatography; (2) bound proteins were eluted with 50 mM ethanolamine at pH 10.8; and (3) fractions were collected and promptly neutralized with a 1/30 volume of 0.5 M NaH_2PO_4, and concentrated to 250–300 μl using an Ultrafree-4 centrifugation unit with a Biomax-30 membrane (UFV4BTK25, Millipore).

The homogeneous dimeric DPPIV/CD26 was isolated by size-exclusion fast protein liquid chromatography (SE-FPLC). The immunopurified DPPIV/CD26 was loaded onto a Superdex 200 column (Pharmacia Biotech), which had been previously equilibrated with PBS, and eluted at a flow rate of 0.5 ml/min with equilibrium buffer. The molecular weight of the obtained protein was determined from the elution profile of standard proteins.

Sample preparation. Droplets (5 μl) of the protein solution were placed on hydrophilized (glow discharge treatment for 30 s at 8 W in a BALTEC MED 020 device from Baltec, Liechtenstein) carbon-coated copper grids and blotted to create an ultrathin layer of the solution. A droplet of 2% (m/v) phosphotungstic acid (PTA) was subsequently applied for 30 s and blotted again. The grids were eventually propelled into liquid ethane at its freezing point (89 K) using a custom made plunging device. Liquid nitrogen was used as storage medium. The specimen preparation procedure was essentially the same as described earlier for the 3D-structure determination of influenza HA [15]. The embedding matrix had a somewhat higher contrast than that of the conventional vitreous-ice preparation. Despite the relatively high acceleration voltage of the microscope (160 kV) and the chosen "close-to-focus" imaging conditions, a better signal-to-noise ratio is obtained and the beam sensitivity is reduced [16]. Comparison of the X-ray crystallographic structure of HA with our three-dimensional EM-reconstruction revealed no significant structural difference within the limits of the achieved resolution of 10 Å.

Cryo-electron microscopy. Vitrified samples were transferred into a Tecnai F20 FEG using a Gatan cryoholder and –stage (Model 626). Samples were constantly cooled by LN2 during imaging to maintain a sample temperature of $T = 93$ K. Imaging was performed at 160 kV accelerating voltage at a defocus value of 600 nm, which corresponds to a first zero of the contrast transfer function at 13 Å ($C_s = 2.0$ mm). Micrographs were recorded following the low-dose protocol of the microscope at a primary magnification of 65,473×.

Image processing. Micrographs were screened using a laseroptical diffractometer. Images were selected for further processing, which were free of aberrations, charging, drift, misalignments, etc. The selected micrographs were then digitized using the Heidelberg "Primescan" drum scanner (Heidelberger Druckmaschinen AG, Heidelberg, Germany) at a resolution of 4 μ (6350 dpi), which corresponds to a pixel resolution of 0.61 Å on the negative.

All subsequent steps of the image processing procedure were performed with IMAGIC 5 software (Image Science GmbH, Berlin, Germany). 11,121 single molecules were interactively selected and used for further processing. The three-dimensional reconstruction was calculated using the "angular reconstitution" approach [17] as described elsewhere [15]. Fourier shell correlation (FSC) [18] of two different 3D reconstructions, each of which included half of the final class averages, was done to assess the resolution at a 0.5 cutoff. For the final reconstruction the resolution was determined to be ~14 Å.

For docking experiments of the crystal structure of POP, the Situs Software Package Version 2.0 (http://situs.scripps.edu/index.html) was used to fit the high-resolution X-ray structure into the EM density maps. The docking procedure was performed following the protocol described by Wriggers and Birmanns [19].

Results and discussion

Homogeneous dimeric DPPIV/CD26 with enzymatic activity was purified and isolated by size-exclusion fast protein liquid chromatography (SE-FPLC) following immunoaffinity chromatography. The elution profile of rat DPPIV/CD26 after SE-FPLC was shown in Fig. 1A. The purity and enzymatic activity of these fractions were analyzed by activity assay (Fig. 1B), polyacrylamide gel electrophoresis under non-denaturing conditions (Fig. 1C), and SDS–PAGE (Fig. 1D) as described previously [14]. As shown by gel electrophoresis (Fig. 1C), dimeric DPPIV/CD26 has a molecular weight of 210 kDa. Fraction 24, which showed homogeneous, dimeric DPPIV/CD26 with the highest enzymatic activity and contained a homogeneous glycan structure of complex form [9], was selected for cryo-transmission electron-microscopic studies.

The three-dimensional structure of this protein was determined at a resolution of ~14 Å applying cryo-electron microscopy and angular reconstitution techniques to single particle preparations. All reconstruction procedures were performed without application of symmetry restraints. The obtained 3D-structure can be described as two distinct, nearly identical barrel-shaped subunits, which are connected by two well-defined

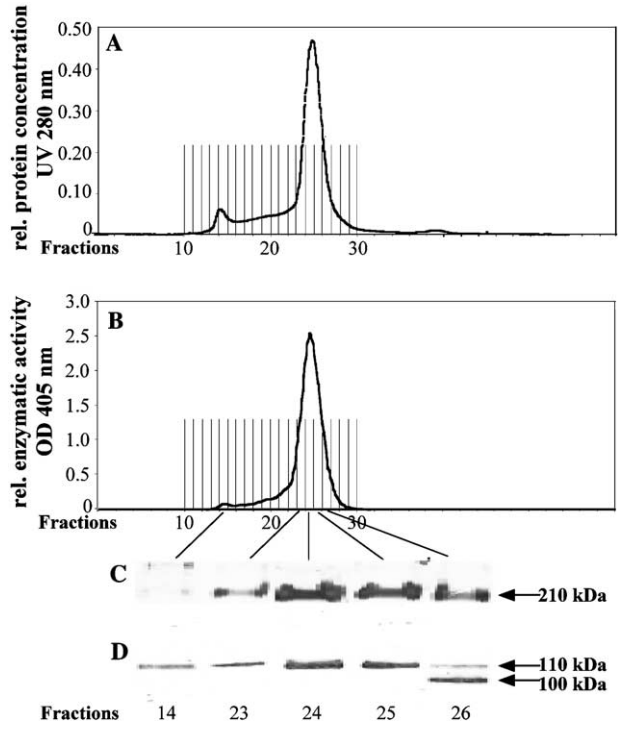

Fig. 1. Isolation and analysis of homogeneous, dimeric rat DPPIV/CD26. (A) Typical elution profile of rat DPPIV/CD26 after size exclusion chromatography on a Superdex 200 column. (B) Analysis of enzymatic activity. (C) Silver stained polyacrylamide gel electrophoresis under non-denaturing conditions. (D) Silver stained SDS–PAGE.

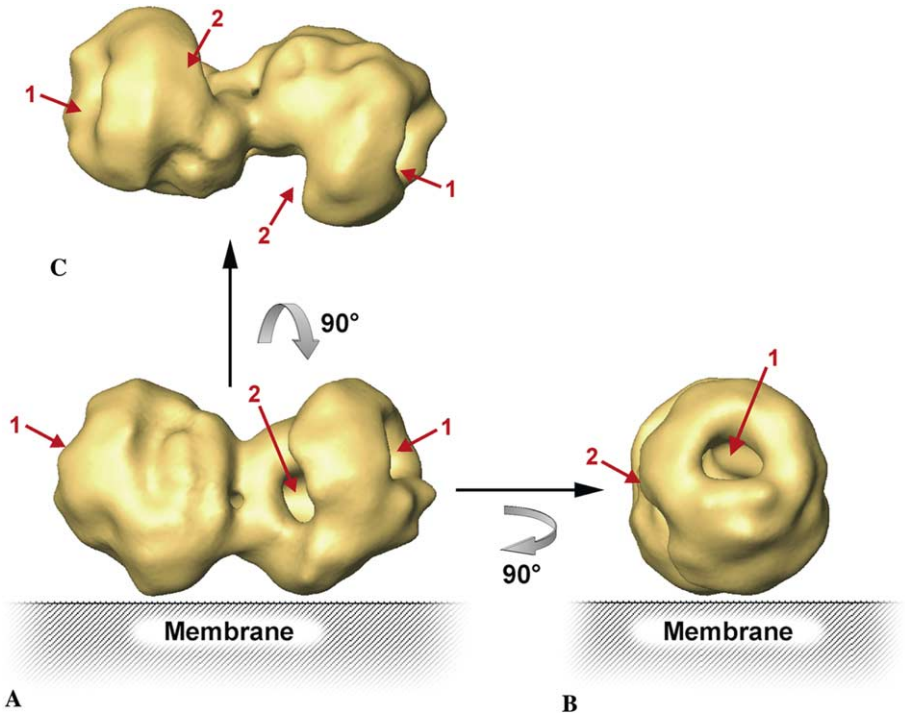

Fig. 2. Surface representations of the 3D-reconstruction of rat DPPIV/CD26 at a resolution of ~14 Å, determined from cryo electron micrographs and single particle analysis. The distal opening (1) and the lateral opening (2) are indicated by red arrows (for further description see text). (A) Side view. (B) Side view rotated (in-plane) by 90°. (C) Top view. The putative localization of the cellular membrane is schematically indicated in (A) and (B).

bridges, confirming the expected dimeric organization of the protein (Fig. 2).

The subunits are tilted against each other at an angle of approximately 120° when the molecule is observed from the side (Fig. 2A). Viewed longitudinally, the subunits are also twisted against each other (Figs. 2B and C). The overall length of the dimer is ~120 Å, whereas the individual monomers measure ~70 Å in length and ~65 Å in diameter. The threshold of the depicted surface representation was chosen to correspond to the experimentally determined molecular weight of 210 kDa. Glycosylated sites in the molecule, which tend to be highly flexible, do not contribute to the density map.

The most prominent features of the reconstruction are two openings observed in each of the two subunits, creating a central channel through each monomer. In its central part each channel widens to form a substantial cavity. One opening (~18 Å diam) is located distally at the outer top face of each monomer, while the second (23 Å diam) is located in the side just below a massive bulge bending from the top. The overall spatial organization, which is noticeably characterized by the preferential alignment of its two subunits towards one side, suggests a plausible orientation in the membrane: if one considers the distal openings to be the entrance or exit sites for the uptake or release of substrates, they should be preferentially directed away from the membrane (Figs. 2A and B).

There are several indications in the literature of close structural analogies of DPPIV/CD26 and prolyl oligopeptidase (POP, EC 3.4.21.26). These findings are based on sequence alignments, structure simulations/models, CD, and FTIR spectroscopy [20,21]. The endopeptidase POP, which cleaves after proline, is also a serine peptidase; like DPPIV/CD26 it possesses a catalytic site consisting of a Gly–X–Ser–X–Gly conserved sequence. Based on the known crystal structure of POP and three-dimensional structure predictions [22,23], the following structural elements are expected for DPPIV/CD26:

(a) a seven-bladed β-propeller domain,
(b) a compact α/β-hydrolase domain including the catalytic triad Ser, His, and Asp (as in POP S554 H680 and D641),
(c) a central cavity, providing space for access of substrates to the catalytic site.

On the basis of these expected structural motifs, we performed docking calculations and tried to fit the density map of the known POP crystal structure (pdb-entry: 1qfm) into our EM-structure. At first sight, the result of this calculation reveals certain similarities, such as the overall dimensions and the general spatial organization (Fig. 3). In particular, the volume of the catalytic domain in POP is in good agreement.

However, there are also several details that are mismatched. The top part of DPPIV/CD26, which is the β-propeller in the POP structure, is clearly larger for

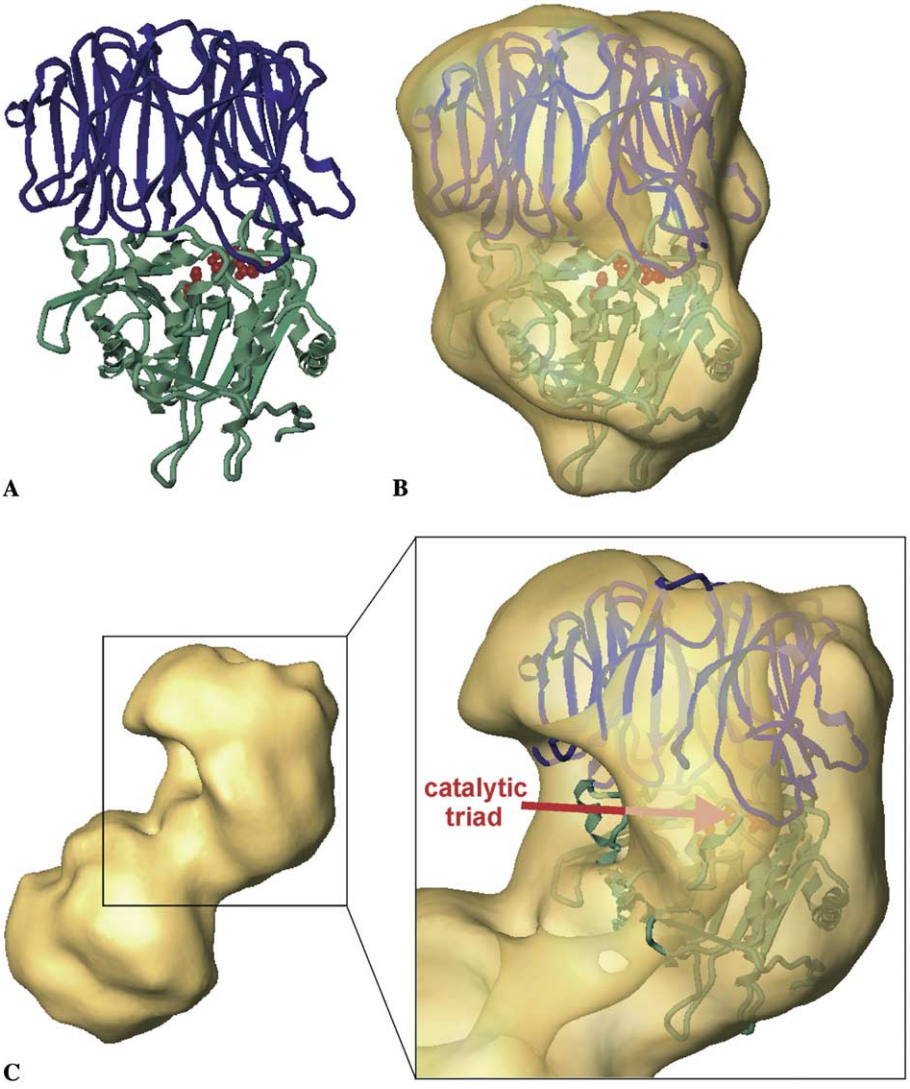

Fig. 3. Crystal structure of the prolyl oligopeptidase (POP) [24] compared with the 3D reconstruction of rat DPPIV/CD26. (A) X-ray structure of POP (pdb-code: 1QFM): The secondary structure of the β-propeller domain and the catalytic domain are shown in blue and green, respectively. The catalytic triad (Ser^{554}, Asp^{641}, and His^{680}) is represented by red balls. (B) X-ray structure of POP as in (A) and coated by a transparent surface representation (yellow). This surface representation is the result of a low-pass filtering of the X-ray-structure and represents a resolution comparable to the EM-reconstruction (14 Å). (C) Surface representation of the 3D reconstruction of the rat dimeric DPPIV/CD26 (left) and 3D structure of the POP (secondary structure representation) docked into one monomer of the DPPIV/CD26 density map by using "Situs" software [19] (right). The resulting location of the catalytic triad is indicated by an arrow.

DPPIV/CD26 (see Fig. 3C) and shows a central opening of diameter 18 Å, whereas the POP analogue is more compact and reveals a very small opening of only 4 Å [24]. The central cavity of DPPIV/CD26 is approximately 1.4 times larger than that of POP. The docking procedure therefore produces a position for the catalytic triad of POP misleadingly located in the cavity of DPPIV/CD26. The catalytic site of DPPIV/CD26 would, in fact, be expected to occupy a more proximal position.

The most striking difference is the second side opening in DPPIV/CD26, which is absent in POP. This new motif, taken together with the above-mentioned mismatches, leads us to speculate that the functionality of DPPIV/CD26 is most probably driven by a different mechanism. If we assume that the catalytic triad is located at the bottom of each subunit cavity, substrates might reach the catalytic center of DPPIV/CD26 by two different routes. By entering from the top, the catalytic triad would be accessible by a direct route leading down to the bottom of the subunit. Alternatively, the substrate might enter through the side opening. In both cases, the products of enzymatic cleavage could be expelled through the complementary opening. This plausible mechanism, based on the obvious spatial organization of DPPIV/CD26, might be more complicated for POP. Since there is no apparent two-way entry/exit mechanism (the 4 Å opening in the propeller is much too small to incorporate a peptide chain), one has to assume that a

sequential opening and closing is necessary. It has been proposed that a certain flexibility of the interface between blade 1 and 7 could be responsible for an active opening and closing. Since the propeller closure is stabilized only by hydrophobic interactions and no velcro has been found, reversible opening is very likely involved in substrate uptake by POP [23,24].

Acknowledgments

The authors gratefully acknowledge the generous support of the *Deutsche Forschungsgemeinschaft* Bonn (Sonderforschungsbereich 449) for the loan of the Tecnai F20 electron microscope (DFG-Großgeräteinitiative), the *Sonnenfeld-Stiftung* and the *Fonds der Chemischen Industrie*, Frankfurt/Main.

Note added in proof. During preparation of the manuscript Rasmussen et al. published the three-dimensional structure of the *human* DPPIV by the use of X-ray diffraction showing this protein to appear in a very similar spatial organization (Nature Structure Biology 10 (2003) 19–25).

References

[1] R. Mentlein, B. Gallwitz, W.E. Schmidt, Dipeptidyl-peptidase IV hydrolyses gastric inhibitory polypeptide, glucagon-like peptide-1 (7–36) amide, peptide histidine methionine and is responsible for their degradation in human serum, Eur. J. Biochem. 214 (1993) 829–835.

[2] I. De Meester, S. Korom, J. Van Damme, S. Scharpe, CD26, let it cut or cut it down, Immunol. Today 20 (1999) 367–375.

[3] C. Morimoto, S.F. Schlossman, The structure and function of CD26 in the T-cell immune response, Immunol. Rev. 161 (1998) 55–70.

[4] A. von Bonin, J. Huhn, B. Fleischer, Dipeptidyl-peptidase IV/CD26 on T cells: analysis of an alternative T-cell activation pathway, Immunol. Rev. 161 (1998) 43–53.

[5] W. Reutter, O. Baum, K. Loester, H. Fan, J.P. Bork, K. Bernt, C. Hanski, R. Tauber, Functional aspects of the three extracellular domains of dipeptidyl peptidase IV: characterization of glycosylation events, of the collagen-binding site and endopeptidase activity, in: B. Fleischer (Ed.), Dipeptidyl Peptidase IV (CD26) in Metabolism and the Immune Response, R.G. Landes Company, Texas, 1995, pp. 55–79.

[6] D. Marguet, A.M. Bernard, I. Vivier, D. Darmoul, P. Naquet, M. Pierres, cDNA cloning for mouse thymocyte-activating molecule. A multifunctional ecto-dipeptidyl peptidase IV (CD26) included in a subgroup of serine proteases, J. Biol. Chem. 267 (1992) 2200–2208.

[7] Y. Misumi, Y. Hayashi, F. Arakawa, Y. Ikehara, Molecular cloning and sequence analysis of human dipeptidyl peptidase IV, a serine proteinase on the cell surface, Biochim. Biophys. Acta 1131 (1992) 333–336.

[8] W.J. Hong, D. Doyle, Molecular dissection of the NH2-terminal signal/anchor sequence of rat dipeptidyl peptidase IV, J. Cell. Biol. 111 (1990) 323–328.

[9] H. Fan, W. Meng, C. Kilian, S. Grams, W. Reutter, Domain-specific N-glycosylation of the membrane glycoprotein dipeptidylpeptidase IV (CD26) influences its subcellular trafficking, biological stability, enzyme activity, and protein folding, Eur. J. Biochem. 246 (1997) 243–251.

[10] H. Fan, J. Dobers, W. Reutter, DPPIV/CD26: structural and biological characteristics of asparagine and cysteine mutants, in: S. Mizutani (Ed.), Cell-surface Aminopeptidases: Basic and Clinical Aspects, Elsevier science, Amsterdam, 2001, pp. 303–316.

[11] J. Dobers, S. Grams, W. Reutter, H. Fan, Roles of cysteines in rat dipeptidyl peptidase IV/CD26 in processing and proteolytic activity, Eur. J. Biochem. 267 (2000) 5093–5100.

[12] S. Ogata, Y. Misumi, E. Tsuji, N. Takami, K. Oda, Y. Ikehara, Identification of the active site residues in dipeptidyl peptidase IV by affinity labeling and site-directed mutagenesis, Biochemistry 31 (1992) 2582–2587.

[13] F. David, A.M. Bernard, M. Pierres, D. Marguet, Identification of serine 624, aspartic acid 702, and histidine 734 as the catalytic triad residues of mouse dipeptidyl-peptidase IV (CD26). A member of a novel family of nonclassical serine hydrolases, J. Biol. Chem. 268 (1993) 17247–17252.

[14] J. Dobers, M. Zimmermann-Kordmann, M. Leddermann, T. Schewe, W. Reutter, H. Fan, Expression, purification, and characterization of human dipeptidyl peptidase IV/CD26 in Sf9 insect cells, Protein Expr. Purif. 25 (2002) 527–532.

[15] C. Böttcher, K. Ludwig, A. Herrmann, M. van Heel, H. Stark, Structure of influenza haemagglutinin at neutral and at fusogenic pH by electron cryo-microscopy, FEBS Lett. 463 (1999) 255–259.

[16] S. De Carlo, C. El-Bez, C. Alvarez-Rua, J. Borge, J. Dubochet, Cryo-negative staining reduces electron-beam sensitivity of vitrified biological particles, J. Struct. Biol. 138 (2002) 216–226.

[17] M. Van Heel, Angular reconstitution: a posteriori assignment of projection directions for 3D reconstruction, Ultramicroscopy 21 (1987) 111–123.

[18] M. Van Heel, G. Harauz, Resolution criteria for three-dimensional reconstructions, Optik 73 (1986) 119–122.

[19] W. Wriggers, S. Birmanns, Using situs for flexible and rigid-body fitting of multiresolution single-molecule data, J. Struct. Biol. 133 (2001) 193–202.

[20] C. Durinx, A.M. Lambeir, E. Bosmans, J.B. Falmagne, R. Berghmans, A. Haemers, S. Scharpe, I. De Meester, Molecular characterization of dipeptidyl peptidase activity in serum: soluble CD26/dipeptidyl peptidase IV is responsible for the release of X-Pro dipeptides, Eur. J. Biochem. 267 (2000) 5608–5613.

[21] A.M. Lambeir, P. Proost, C. Durinx, G. Bal, K. Senten, K. Augustyns, S. Scharpe, J. Van Damme, I. De Meester, Kinetic investigation of chemokine truncation by CD26/dipeptidyl peptidase IV reveals a striking selectivity within the chemokine family, J. Biol. Chem. 276 (2001) 29839–29845.

[22] W. Brandt, Development of a tertiary-structure model of the C-terminal domain of DPP IV, Adv. Exp. Med. Biol. 477 (2000) 97–101.

[23] M.D. Gorrell, V. Gysbers, G.W. McCaughan, CD26: a multifunctional integral membrane and secreted protein of activated lymphocytes, Scand. J. Immunol. 54 (2001) 249–264.

[24] V. Fulop, Z. Bocskei, L. Polgar, Prolyl oligopeptidase: an unusual beta-propeller domain regulates proteolysis, Cell 94 (1998) 161–170.